Spectral Signatures of Intramolecular Charge Transfer Process in β-Enaminones: A Combined Experimental and Theoretical Analysis

ARTICLE *in* THE JOURNAL OF PHYSICAL CHEMISTRY B · AUGUST 2009

Impact Factor: 3.3 · DOI: 10.1021/jp9009542 · Source: PubMed

5 AUTHORS, INCLUDING:

Ramprasad Misra
Weizmann Institute of Science
13 PUBLICATIONS **72** CITATIONS
SEE PROFILE

Abhijit Mandal
13 PUBLICATIONS **231** CITATIONS
SEE PROFILE

Madhuri Mukhopadhyay
Jawaharlal Nehru Centre for Advanced Sci…
16 PUBLICATIONS **74** CITATIONS
SEE PROFILE

Spectral Signatures of Intramolecular Charge Transfer Process in β-Enaminones: A Combined Experimental and Theoretical Analysis

Ramprasad Misra,[†] Abhijit Mandal,[†,§] Madhuri Mukhopadhyay,[†] D. K. Maity,[‡] and S. P. Bhattacharyya*[,†]

Department of Physical Chemistry, Indian Association for the Cultivation of Science, Jadavpur, Kolkata 700032, India, and Theoretical Chemistry Section, Chemistry Group, Bhabha Atomic Research Centre, Mumbai 400085, India

Received: February 2, 2009; Revised Manuscript Received: June 16, 2009

In this paper, we present spectroscopic signatures of intramolecular charge transfer (ICT) and effects of solvent on the ICT process in 3-(phenylamino)-2-cyclohexen-1-one (PACO), a member of the well-known molecular family, the β-enaminones. The dual fluorescence in the steady state emission spectra of the molecule in polar solvents indicates the occurrence of ICT, which is further supported by time-resolved studies, using time correlated single photon counting technique with picosecond resolution. To understand the nature of the charge transfer, pH dependent studies of the probe in water were performed, where a quenching of fluorescence was observed even in the presence of very low concentrations of acids. Solvent induced fluorescence quenching was observed in ethanol and methanol. The ICT process was also investigated by quantum chemical calculations. To understand the role of solvents in the ICT process, we have theoretically studied the macroscopic and microscopic solvation of the probe in water. The absorption spectra of the molecule in the gas phase as well as in water were simulated using time dependent density functional theory with cc-pVTZ basis set and self-consistent reaction field theory that models macroscopic solvation. The possibility of microscopic solvation in water was probed theoretically and the formation of 1:3 molecular clusters by PACO with water molecules has been confirmed. Our findings could have a bearing on pH sensing applications of the probe.

1. Introduction

Charge transport over long distances in organic molecules has significant application in the molecular electronics and organic photovoltaics.[1] The charge transfer or the electron transfer process in organic molecules has been studied widely as it is a key step in many biological processes, including metabolism and photosynthesis.[2] Understanding the mechanism of charge transfer and its applications continues in intense areas of research.[3−10] It is a well-known fact that a donor and an acceptor, connected through an electron bridge in a molecule, endow it with the possibility of intramolecular charge transfer, either in the ground state or in the excited state.[11] Donor−acceptor systems of this type stabilize the molecules significantly, imparting thermal stability to the molecule and creating the potentiality of nonlinear optical (NLO) response.[12] There are a number of issues concerning the mechanism of the intramolecular charge transfer (ICT) process that have remained hitherto unsolved,[13−15] despite many experimental investigations and theoretical calculations. Initially, the twisted intramolecular charge transfer (TICT) mechanism[14−16] appeared to be the most acceptable mechanism. Later on, Yoshihara et al.[17] showed that a loosely connected donor−acceptor molecule and its planar analogue shows the same intensity of charge transfer. Thus, they refuted the idea of the importance of twisted state of the molecule in the ICT process and proposed planar intramolecular charge transfer (PICT) mechanism. There are other literature references that also support the fact that for charge transfer the molecule need not be twisted.[18,19] While considering the excited state charge transfer phenomenon, one may not fail to take note of a charge transfer process that stands in sharp contrast with the ICT process. The process referred to has been known as the intramolecular proton transfer (IPT) process. Compared to the ICT, IPT is a much faster process. In IPT, the excited state lifetime of the probe is of the order of 10 ps in contrast with the order of 100 ps to 10 ns in the case of ICT.[20−22] The IPT phenomenon also demands a minimum distance condition between the loosely bound proton donor and the proton acceptor groups.[23] The ICT process, on the other hand, can occur over much longer distances. The ICT process polarizes electronic charge distribution within the probe which brings in solvation. The solvation often helps in stabilizing the ICT state by macroscopic solvent polarization, that is, by the solvent acting as a dielectric continuum, or by microscopic solvation, that is, by specific interaction between the solvent and the probe leading to cluster formation, or by both. Studying the structure and the reactivity of microsolvated molecules, popularly known as "molecular clusters", has been an intense area of research.[24−29] The properties of these clusters vary notably from those in the gas phase. Studying a system of this type helps one understand the solvent induced effects in different complex reactions. Understanding the origin of such variations could lead to better understanding of the roots of molecular recognition, which is an important process in living systems.[27,28] The choice of water as a solvent is important as it serves as the solvent for many biological systems.[30] The study of specific interactions of a probe with water has important bearing on the understanding of mechanisms of complex reactions and designing of new drugs.[27−29]

* To whom correspondence should be addressed. Fax: +91 3324732805. E-mail: pcspb@iacs.res.in.
[†] Indian Association for the Cultivation of Science.
[‡] Bhabha Atomic Research Centre.
[§] Present address: Sol−Gel Division, Central Glass and Ceramic Research Institute, Jadavpur, Kolkata-700032, India.

10.1021/jp9009542 CCC: $40.75
Published on Web 07/13/2009

β-Enaminones (or, β-enamino ketones) are well-known for their usefulness in synthetic organic chemistry as precursors to many bioactive natural products.[31−33] The synthetic utility of those molecules in the synthesis of dopamine autoreceptor agonists, anticonvulsants, and one part of the side chain of an anticancer drug, Taxol, have been reported.[30−35] Search for new methodologies[36−40] for the syntheses of β-enaminone is a topic of considerable volume of research in synthetic organic chemistry but little seems to be known about the spectroscopic properties of these molecules.

The question addressed in this paper concerns the spectral signatures of the ICT process in 3-(phenylamino)-2-cyclohexen-1-one (PACO). The layout of the paper is as follows. In section 2, we present the experimental and theoretical techniques adopted. The recorded absorption spectra in different solvents are presented in section 3a while in section 3b the gas phase absorption spectrum of the molecule computed by ab initio theoretical procedure along with the computed spectrum in water as solvent is presented. In section 3c, we present the experimentally recorded emission spectra of the molecule in different solvents in room temperature. In section 3d, the excitation wavelength dependent spectra of the molecule are presented. Section 3e deals with the effects of acids and bases on absorption and emission spectra of the molecule. In section 3f, the results of low temperature fluorescence and phosphorescence spectral studies are discussed. In section 3g, a thorough analysis of the results obtained from time dependent study is made and some inferences are drawn about the ICT process in the molecule concerned. The experimentally observed oscillator strength of absorption and emission in different solvents are presented in section 3h. The radiative rate constants of absorption and emission of the probe in different solvents are also presented. Section 3i deals with the excited state optimized geometry of the molecule, calculated by Austin Model 1 (AM1) level[41] of calculations.

2. Materials and Methods

2a. Experimental Techniques. ***i. Synthesis of the Molecule and Steady-State Spectroscopic Studies.*** The molecule 3-(phenylamino)-2-cyclohexen-1-one was synthesized using the procedure described in ref 38. An equimolar mixture of 1,3 -hexane-dione and aniline was used as the starting material. The reaction was completed in minutes under inert (N_2) atmosphere at room temperature in acetonitrile solvent in the presence of a catalytic amount of cerium(IV) ammonium nitrate (20 mol %). The crude product was washed with doubly distilled water and brine and dried over $MgSO_4$. The product was purified by column chromatography over silica gel (120 mesh) using 50% ethyl acetate/petroleum ether solution. The structure was confirmed through ^{1}H and ^{13}C NMR and IR spectra of the molecule. The spectral characterization data of the PACO is as follows: ^{1}H NMR (300 MHz, $CDCl_3$, in ppm): δ 1.78−1.82 (m, 2H), 2.20 (t, 2H), 2.45 (t, 2H), 5.44 (s, 1H), 6.93−7.22 (m, 5H), 8.53 (brs, 1H); ^{13}C NMR (75 MHz, $CDCl_3$, in ppm): δ 21.3, 28.9, 35.2, 97.5, 123.8, 125.4, 128.8, 137.6, 166.0, 198.4 and IR (KBr, in cm^{-1}) 3261, 2941, 1595, 1571, 1527, 1492, 1425, 1244, 1180, 702.

The steady state electronic absorption and emission spectra of the PACO were recorded in different solvents with a wide range of polarity ($\varepsilon = 2-80$) on a Shimadzu UV−vis recording spectrophotometer UV-2401 (PC) S220 V and Fluoro Max 3 (Jobin Yvon Horiba) fluorimeter, respectively. The solvents were of spectroscopic grades (Merck/Spectrochem) with reported water content at 0.03−0.05% level. Acetonitrile was refluxed with P_2O_5 for 4 h, decanted off, and fractionally distilled to get absolutely water free solvent. Dimethyl sulfoxide (DMSO) was dried by keeping it over calcium hydride (CaH_2) for 12 h and then fractionally dried over CaH_2 under reduced pressure. The distilled DMSO was kept over type 4A molecular sieves. Methanol was dried by fractional distillation over type 3A molecular sieves. Triply distilled water was used to prepare all aqueous solutions and was checked for residual fluorescence, if any, before use. We have studied the excitation wavelength dependent emission spectra of the molecule in different solvents by exciting the molecule with light of different wavelengths ($\lambda_{ex} = 280-360$ nm). The absorption and emission spectra of the PACO were recorded in the presence of micromolar concentrations of a strong base (NaOH) and a strong acid (HCl). The excitation spectra of the molecule in solvents with different polarity were also recorded. The quantum yields in different solvents were measured by following the standard procedure.[42] To avoid the effect of concentration, very dilute solutions were taken for quantum yield measurement of the probe. The low temperature (77 K) emission spectra of the molecule in 3-methyl-pentane and ethanol glass matrix were recorded on a HITACHI spectrophotometer model F4500. For this purpose a small quartz Dewar was used which was fitted to the aforesaid instrument. The phosphorescence of the molecule was recorded at 77 K using the same spectrometer. A rotary chopper was used to collect the phosphorescence. The low temperature environment was produced by using liquid nitrogen as the coolant. Except for the low temperature study of the probe, all other spectral data were collected at an ambient temperature of 23 °C.

ii. Time Resolved Measurements. The lifetimes of the probe in different solvents have been recorded by using time correlated single photon counting (TCSPC) technique in a HORIBA JOBIN YVON instrument. The system was excited at 295 nm by using picosecond diode laser (IBH Nanoled-07). The detector was a Hamamatsu MCP plate photomultiplier (R3809U). The single photon counting technique comprised an Ortec 9327 discriminator (CFD, Tenelec TC 454) and Fluoro Hub Single Photon Counting controller. The data were collected with a DAQ card as a multichannel analyzer. The spectra obtained were analyzed by using the Software DAS6 at Data Station v2.3 through exponential fitting yielding the corresponding lifetimes. The quality of fit was judged in terms of a Durbin−Watson (DW) parameter, weighted residuals, and reduced χ^2 values.

2b. Theoretical Calculations. ***i. Semiempirical Calculations.*** Semiempirical calculations were done by using closed shell restricted Hartree−Fock (RHF) theory at the AM1 level of approximation by using a standard package, MOPAC97 version 6.0 for windows. RHF was employed to find the optimized geometry of the molecule in the ground state which was further refined by configuration interaction (CI) calculation. The excited state geometry was fully optimized by configuration interaction calculation in which all the states involving the highest occupied molecular state (HOMO) and lowest unoccupied molecular state (LUMO) were used. The dipole moments of the molecule at the optimized ground and excited state geometries were also calculated.

ii. Ab-Initio Calculations. At the ab initio level all the calculations were performed using the quantum chemistry software package GAMESS.[43] PC-based Linux platform was used for all the calculations. The visualization of the optimized structures was done by using the MOLDEN[44] software. The B3LYP DFT functional was used for the calculation of the ground state electronic structure of the molecule with cc-pVTZ correlated basis set. TD-DFT calculations were done for

SCHEME 1: Structure of PACO. The Numbering of Only the Heavy Atoms Is Done for Reference

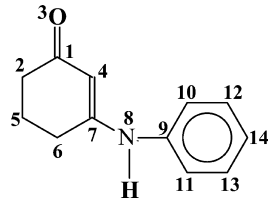

predicting the absorption spectrum by using the B3LYP functional with the same set of basis functions. Since ICT molecules have been reported to be inadequately described by the B3LYP functional, all the calculations were repeated with the mPW1PW91 functional, which has been known to be more reliable in describing charge transfer.[45] Macroscopic solvent polarization effect has been taken into account by invoking the self-consistent reaction field (SCRF) model. The SCRF cavity radius was set equal to 5.41 and 5.42 Å for bare probe molecule and 1:3 PACO−water cluster, respectively, from the computed end to end distance of the relevant molecular species. For water, microscopic or specific interaction with solvent molecules was taken into account by studying 1:n (n = 3) clusters of PACO with water. For the simulation of absorption spectra of the molecule, we have considered vertical transitions involving the lowest 10 excited states of the molecule. The simulation of the UV/vis spectra was carried out considering the full-width at half-maximum (fwhm) as an empirical parameter for each transition. By trial and error, fwhm was fixed at 100 nm for the best fit. The absorption profile was calculated from the sum of all the bands by applying the Gaussian model. The total integrated intensity under the absorption profile was kept equal to the sum of all the oscillator strengths. TDDFT calculations were performed with the AM1/CI optimized excited state geometry using the mPW1PW91 functional and cc-pVTZ basis set for computing transition energies and oscillator strength at the relaxed excited state geometry.

3. Results and Discussions

3a. Absorption Spectrum of PACO. The recorded absorption spectra of the probe molecule (Scheme 1) in methyl cyclohexane (the molar extinction coefficient at absorption maxima, $\varepsilon_{max} \approx$ 11700 mol^{-1} dm^3 cm^{-1}), isopropyl alcohol, DMSO ($\varepsilon_{max} \approx$ 12000 mol^{-1} dm^3 cm^{-1}), methanol ($\varepsilon_{max} \approx$ 10600 mol^{-1} dm^3 cm^{-1}) and water ($\varepsilon_{max} \approx$ 10450 mol^{-1} dm^3 cm^{-1}) are shown in Figure 1. The concentrations of solutions were in the range 2.00−2.25 $\times$ 10^{-3} mol dm^{-3}. In the steady state spectra, the absorption maxima of the molecule appear at 295, 305, and 307 nm in methyl cyclohexane, methanol, and water, respectively. The red-shift observed in the absorption spectra of the molecule in solvents with higher polarity indicates progressively greater stabilization of the excited state in polar environment. We anticipate that the red-shift is a signature of intramolecular charge transfer in the probe molecule upon excitation. The absorption maxima of the molecule in different solvents are reported in Table 1. The dielectric constants and hydrogen-bond donor abilities of the solvents used are also displayed in the same table. The solvent polarity appears to be one of the important factors that determine the stabilization of the excited state. Specific interactions also do appear to play a vital role.

3b. Theoretical Prediction of Structure and Absorption Spectrum of PACO. The absorption spectrum of given β-enaminone has been computed by TDDFT (B3LYP) and TDDFT (mPW1PW91) methods. The calculations have been performed with the GAMESS suite of program. Optimization of the ground state geometry have been done with B3LYP/cc-pVTZ as well as mPW1PW91/cc-pVTZ methods. Four sets of calculations were performed.

(i) The geometry of the bare molecule in the gas phase was optimized. The predicted values of important geometrical parameters are reported in Table 2a (i). TDDFT calculation has been performed at this geometry and the computed absorption spectrum of the bare molecule is shown in figure 2 (solid line). Compared to the experimental absorption spectrum of the probe in methyl cyclohexane, which is an extremely nonpolar solvent, the theoretical spectrum of the bare molecule is considerably blue-shifted.

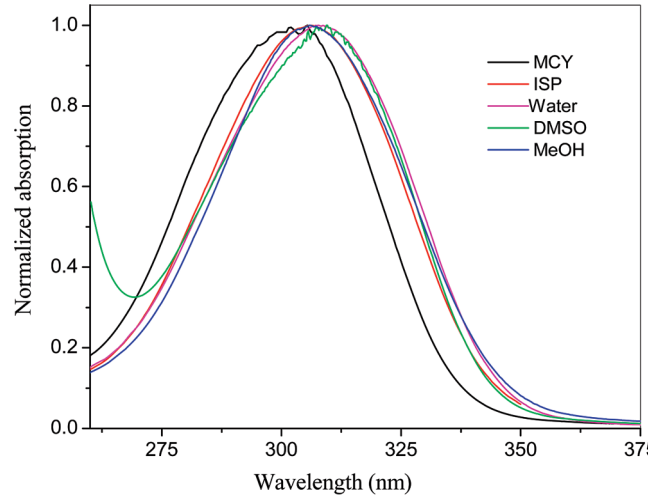

Figure 1. The normalized absorption spectra of PACO in methyl cyclohexane (MCY), methanol (MeOH), isopropyl alochol (ISP), DMSO, and Water.

TABLE 1

(1a) The room temperature recorded absorption maxima (λ_{abs}) and emission maxima (λ_{emm}) and quantum yields of emission from locally excited state (ϕ_{LE}) and from the intramolecular charge transfer emission (ϕ_{ICT}) of the probe in different solvents. The dielectric constant (ε) and hydrogen bond donor ability (β) of different solvent are also reported

solvent	ε	β^a	λ_{abs} (nm)	λ_{emm} (nm)	ϕ_{LE}	ϕ_{ICT}
methyl cyclohexane	1.9		295	334	0.006	
1,4-dioxane	2.1	0.0	302	349		
isopropanol	19.9	0.76	307	372		
acetonitrile	37.5	0.19	307	360	0.004	
ethanol	24.6	0.83	307	346, 431	0.009	0.004
methanol	32.7	0.93	305	370, 440	0.015	0.008
DMSO	46.0	0.0	307	365, 430	0.002	0.001
water	80.0	1.17	306	380, 455	0.0011	0.0014

(1b) The absorption (λ_{abs}) and emission maxima (λ_{emm}) of the probe at room temperature in water in absence and presence of micro molar concentrated acid (HCl) of very low concentration (A1) and little higher concentration (A2) and dilute base (NaOH)

medium	λ_{abs}(nm)	λ_{emm}(nm)
water	307	380, 455
water + dilute acid (A1)	302	395, 465
water + dilute acid (A2)	298	385, 475
water + dilute base	307	355, 457

[a] The hydrogen bond donor ability of a solvent, taken from ref 49 by Kamlet et al.

TABLE 2

(2a) The computed distances (in Å) between the pairs of atoms in the probe molecule (PACO) in (i) gas phase, (ii) molecule with water in SCRF ($\varepsilon = 80$) using a SCRF radius of 5.31 Å, (iii) gas phase including three water molecules, and (iv) 1:3 cluster of the molecule and water solvated by water at the SCRF level ($\varepsilon = 80$) using a SCRF radius of 5.32 Å, calculated using TDDFT and cc-pVTZ basis set employing B3LYP and mPW1PW91 functionals in GAMESS. Ground state structure parameters calculated using AM1/CI procedure is also reported for comparison

system and functional uses	C1−O3	C1−C4	C4−C7	C7−N8	N8−C9
		(i) PACO			
B3LYP	1.222	1.454	1.357	1.373	1.408
mPW1PW91	1.217	1.451	1.354	1.366	1.401
AM1	1.23	1.46	1.36	1.39	1.41
		(ii) PACO + SCRF			
B3LYP	1.225	1.450	1.361	1.368	1.411
mPW1PW91	1.221	1.446	1.357	1.362	1.403
		(iii) PACO.3H_2O			
B3LYP	1.244	1.433	1.366	1.360	1.411
mPW1PW91	1.239	1.429	1.363	1.353	1.403
		(iv) PACO.3H_2O + SCRF			
B3LYP	1.253	1.420	1.382	1.345	1.418
mPW1PW91	1.248	1.417	1.378	1.340	1.410

(2b) The computed Mullicken charges in atomic unit (a.u.) on the designated atoms of PACO participating in the charge transfer in (i) gas phase, (ii) molecule with water in SCRF ($\varepsilon = 80$) using a SCRF radius of 5.31 Å, (iii) gas phase including three water molecules, and (iv) 1:3 cluster of the probe molecule and water solvated by bulk water at the SCRF level ($\varepsilon = 80$) using a SCRF radius of 5.32 Å, calculated using TDDFT theory and cc-pVTZ basis with B3LYP and mPW1PW91 functionals in GAMESS (charges on hydrogen summed into heavy atoms were used)

systems and functionals used	C1	O3	C4	C7	N8
		(i) PACO			
B3LYP	0.200668	−0.321813	−0.122923	0.124640	−0.022644
mPW1PW91	0.204691	−0.324733	−0.128953	0.117996	−0.021427
		(ii) PACO + SCRF			
B3LYP	0.206062	−0.328780	−0.128171	0.120324	−0.022788
mPW1PW91	0.203946	−0.328728	−0.128458	0.115897	−0.019174
		(iii) PACO.3H_2O			
B3LYP	0.254561	−0.435221	−0.126631	0.117711	0.002376
mPW1PW91	0.260273	−0.438041	−0.134949	0.116553	0.004236
		(iv) PACO.3H_2O+SCRF			
B3LYP	0.258874	−0.430615	−0.146085	0.116773	0.005590
mPW1PW91	0.261098	−0.433185	−0.150421	0.115383	0.009342

(ii) The geometry of the molecule in the ground state has been reoptimized in water as solvent using the continuum self-consistent reaction field (SCRF) model of solvation. The predicted values of important geometrical parameters are reported in Table 2a (ii). The predicted absorption spectrum including the effects of macroscopic solvent polarization is shown in Figure 2 (dotted line). Compared to the bare molecule, there is a strong red shift in the computed spectrum, although it is still slightly blue-shifted relative to the experimentally observed spectrum in water.

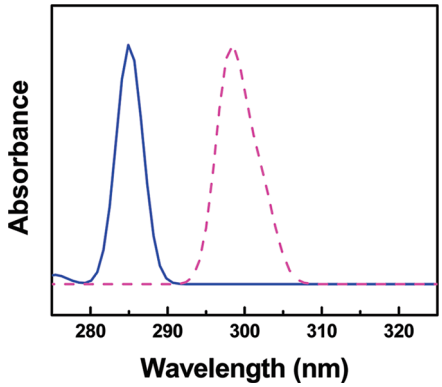

Figure 2. The simulated absorption spectra of PACO, calculated employing TDDFT using cc-pVTZ basis set for gaseous molecule (solid line) and in SCRF [$\varepsilon = 80$] (dotted line).

(iii) Since a water molecule can enter into the formation of hydrogen bond with the probe molecule, we thought it worthwhile to check if microscopic or specific solvation in water takes place and if so, how it affects the structure of the probe and its absorption spectrum. A preliminary search indicates that the molecule forms a 1:3 cluster with water molecule. Figure 3a displays the corresponding equilibrium geometry of the probe solvated by water. The important geometrical parameters are summarized in Table 2a (iii). The computed absorption spectrum of the solvated probe is displayed in Figure 3c (solid line).

(iv) A final calculation was done using the 1:3 cluster formed by the probe with water molecules by allowing the 1:3 PACO−water cluster to interact with water modeled as a continuum through SCRF calculation. It essentially allows the probe molecule to experience both macroscopic and microscopic solvation, which may not always produce the same kind of effects. The predicted structure is displayed in figure 3b and the important structural parameters are reported in Table 2a (iv). The computed absorption spectrum of the microscopically as well as macroscopically solvated β-enaminone in water is exhibited in figure 3c (dotted line). The computed absorption spectrum agrees well with the experimentally recorded spectrum in water.

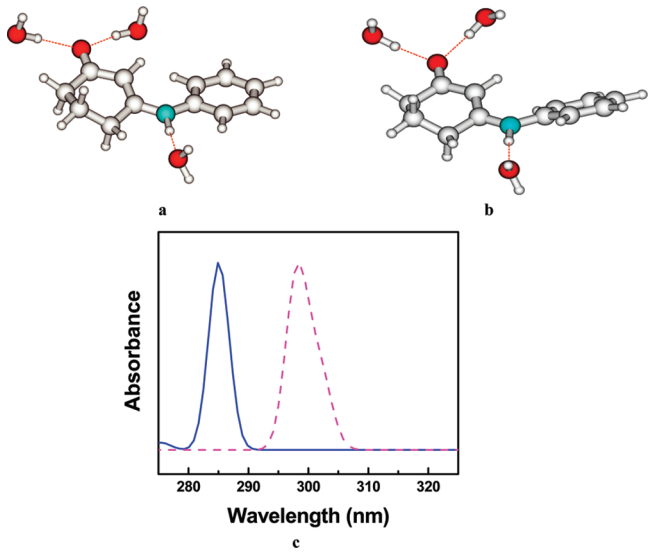

Figure 3. Ground state optimized geometry of PACO including three water molecules in gas phase (a) and using SCRF [ε=80] model (b). The corresponding simulated absorption spectra of the molecule is shown (c) as solid line for gaseous cluster and dotted line for the cluster into the reaction field of water (SCRF) model.

The bond lengths reported in Tables 2a (i−iv) indicate that solvation, both macroscopic and microscopic, tend to stabilize the charge-polarized structure progressively. Thus, the C1−C4 bond length becomes shorter, C1−O3 and C4−C7 bonds become longer, and C7−N8 bond gets shorter as we move along i to iv, taking care of solvation more and more completely. In Table 2b, we have reported the computed charges on the atoms of PACO, participating in charge transfer. The charges were calculated using TDDFT for systems i−iv employing the cc-pVTZ basis set using B3LYP and mPW1PW91 functionals. The two functionals lead to comparable results. As we go from system i to system iv, the positive charge density over C1 and N8 atom increases, whereas we find an increase in negative charge density over the O3 atom while going from system i to system iv. We have compared in Table 3 the results of calculation of transition energies with B3LYP and mPW1PW91 functional and cc-pVTZ basis set, wherein the computed oscillator strengths and the dominant orbital compositions of each transition are also included. The state arising from dominantly HOMO−LUMO transition has the maximum oscillator strength in each case; however, it is not the lowest energy transition except in PACO.3H_2O complex as predicted by TDDFT (B3LYP) calculations. Its position in the energy scale is rather sensitive to solvation.

3c. Room Temperature Emission Spectrum of the Probe. The emission spectra of PACO in different solvents are shown in Figure 4a. We have reported the recorded emission maxima of the molecule in Table 1 for ready reference. Two features can be immediately noted.

(i) There is a large Stoke's shift in the emission maximum (334−355 nm vis-à-vis 290−307 nm) and the shift depends on solvent polarity.

(ii) In polar protic solvents as well as in DMSO, there is dual emission with a new peak appearing in the 430−455 nm region. The dual fluorescence in solvents of high polarity (large dielectric constants) indicates that a new species is formed upon excitation in such solvents.

The occurrence of dual fluorescence from a fluorophore is a well-studied phenomenon.[46,47] The two peaks of the dual fluorescence are generally assigned to the locally excited (LE) state of the molecule and the ICT species formed in the excited state. It is well-known that molecules with a donor and an acceptor moiety in conjugation can emit fluorescence from two relaxed singlet excited states, giving rise to dual fluorescence.[17,48] It is possible that upon photo excitation, the LE state is formed and from it another state (the ICT state) with larger dipole moment is generated. The other possibility is that two species are present in the ground state itself, one being the neutral probe molecule and the other being the protonated cation formed by interaction with traces of water present in the solvents used. The excitation spectrum of PACO, however, does not support this hypothesis. The excitation spectrum of the probe in water with two monitoring wavelengths (360 and 450 nm) are reported in Figure 4b. When monitored at 360 nm, the excitation spectrum in water matches with the absorption spectrum in the same solvent, indicating that the species responsible for the 360 nm emission originates directly from the ground state. When monitored at 450 nm the peak of the excitation spectrum appears at 375 nm and does not juxtapose with the absorption spectrum of PACO, indicating that the ICT emission does not appear directly from the ground state species. The solvents as already described were processed for removing the traces of water so that formation of the protonated cation in the ground state can be discounted. In all probability, therefore, the longer wavelength component of the dual fluorescence originates from a new species generated in the excited state. The considerable red shift in the excitation spectra (vis-à-vis, the absorption spectrum) indicates that the emitting state is very different from the state seen in absorption. In the room temperature emission spectra of the molecule under investigation, we note that the relative intensities of the two emission peaks of the dual fluorescence in ethanol, methanol, and water as solvents show characteristics that are expected on the basis of polarity of solvents. In ethanol, when excited at 290 nm, the emission shows a relatively higher intensity of the 350 nm band than the 430 nm one. The relative intensity ratio was found to decrease in methanol under the same condition. In water, the second peak, that is, the 450 nm peak predominates over the 360 nm peak. From these observations, it is evident that the component corresponding to the emission peak around 450 nm is much more stabilized in solvents with high dielectric constant, viz., methanol and water. It is important at this point to ponder if H-bond donor ability of the solvent also plays a role in stabilizing the ICT state. Hydrogen bond donor abilities of isopropyl alcohol, methanol, ethanol, and water, as determined by Kamlet et al.[49] are 0.76, 0.83, 0.93, and 1.17, respectively. As shown in Table 1a, although the hydrogen bond donor ability of DMSO is 0.0, it has stabilizing influence on the ICT state. It appears therefore that hydrogen bond donor ability of the solvent is not the controlling factor that determines the stabilization of the excited state. The dielectric constant seems to be the key factor that largely determines the stabilization of the ICT species. It is possible to interpret the results schematically as shown in Scheme 2 where the molecule is seen to absorb light and undergo transitions from the ground state (GS) to excited (vertical) electronic state (S_2), which quickly and nonradiatively rearranges to the S_1-LE and the S_1−ICT states of lower energy, from where emissions occur (Scheme 2).

We will explore later if the formation of greater amount the long wavelength component in polar solvents could also be further supported by time-resolved spectroscopy. The quantum yields of the probe in different solvents have been reported in Table 1a. As we have observed dual fluorescence, the LE and ICT quantum yields are reported separately. The quantum yield

TABLE 3: The Vertical Transition Maxima (in nm) and Oscillator Strengths of Different Transitions as Predicted by TDDFT Employing cc-pVTZ Basis Set (both B3LYP and mPW1PW91 Functionals) in GAMESS. Here, H = HOMO, [H − 1] = [HOMO − 1], L = LUMO, [L + 1] = [LUMO + 1], etc.

		transition maxima (nm)		oscillator strength	
systems	dominant transitions	B3LYP	mPW1PW91	B3LYP	mPW1PW91
(i) PACO	[H −1]−L[a]	329.70	318.48	0.0014	0.0016
	H−L[b]	287.62	281.34	0.4567	0.4610
(ii) PACO + SCRF	[H −1]−L[c]	331.68	320.14	0.0011	0.0012
	H−L[d]	287.80	281.54	0.4540	0.4587
(iii) PACO.3H_2O	H−L[e]	298.65	286.41	0.4021	0.4723
	[H −1]−L[f]	295.12	290.41	0.1557	0.0933
(iv) PACO.3H_2O + SCRF	[H −1]−L[g]	305.93	305.61	0.0133	0.0177
	H−L[h]	292.21	293.79	0.4956	0.5031

Contribution of transitions. [a] [H − 1] − L (65%, 64%). [b] H−L (63%, 64%). [c] [H − 1] − L (34%, 26%). [d] H−L (55%, 59%). [e] H−L (65%, 63%). [f] [H − 1]−L (57%, 60%). [g] [H − 1]−L (63%, 63%). [h] H−L (62%, 62%). The numbers in the parentheses represent the percentage of contribution, computed from the B3LYP and mPW1PW91 functionals, respectively.

of the probe decreases from methyl cyclohexane to acetonitrile, while it is higher in alcoholic solvents than in acetonitrile possibly due to decrease in emission through the nonradiative channels. The quantum yield decreases further in water.

3d. Excitation Wavelength Dependent Emission Spectra. The recorded excitation wavelength dependent emission spectra of the probe molecule at room temperature in solvents of varying polarities are displayed in Figure 5a−c. With variation in the excitation wavelength, different emission spectra were obtained. In polar solvents, in which dual fluorescence was observed, a change in the intensity ratio of the emissions from the two species is the key observation. There are minor changes in the positions of the emission peak in some of the solvents while the peak position remains unchanged in others. The position of the emission peak in 1,4-dioxane, for example, is essentially excitation wavelength independent, although the intensity of the emission spectrum decreases with increase in excitation wavelength (Figure 5a). In ethanol, methanol, and water, the excitation wavelength dependent spectra show an interesting behavior in that the first emission peak, which appears between 340 and 380 nm depending on the solvent, disappears when the probe is excited at 320 nm or higher wavelengths. Excitation above the indicated wavelength is accompanied by a sharp increase in the intensity of the second peak, which supposedly originates from the ICT species. The band maxima lie in the 435−455 nm region, depending on the solvent. The emission spectra of the probe for different excitation wavelengths in ethanol and water are shown in Figure 5 panels b and c, respectively. The mentioned spectral features lend further credibility to the suggestion that a new species is formed in the excited state. The observed features are curious and can be explained qualitatively in different ways. It is possible that excitation at shorter wavelength populates a higher excited state (S_2, $\pi-\pi^*$), which has a conical intersection with the LE and the associated ICT state.[50,51] Excitation at shorter wavelengths could therefore populate both the LE and the ICT states. The intensity of the emission is distributed between the LE and the ICT species. Excitation at longer wavelengths (longer than 320 nm), however, populates the LE state directly which rearranges to the ICT state. If the LE → ICT transformation is fast, the emission from the ICT species would increase in intensity as actually observed for longer wavelength excitations. Moreover, we may argue that the energy required to excite a solvated polar probe in a polar solvent would be a function of solvent orientation.[52] At smaller excitation energies, only a small fraction of the total fluorophore populations which are surrounded by the solvent dipole will be excited, leading to smaller emission intensities from the LE species. Some high energy components of the total emission will be missing, which could even give rise to a small red-shift. Actually for excitation above 320 nm and up to the absorption maximum of the S_0-S_1 transition, we observe increased intensity of the ICT band and a decrease in intensity of the LE band.

3e. pH Dependent Emission Study of the Probe. The structure of a probe and the charge redistribution in the excited state has been a matter of potential interest to the scientific community.[53−56] To understand the mechanism of the charge transfer, or, more precisely, the distribution of the electron density among the atoms in the molecule in the ground and excited states, the pH dependent absorption and emission spectral study of the probe has been undertaken at room temperature. The recorded absorption and emission spectra of the probe in water of different pH are displayed in Figure 6 panels a and b, respectively. The probe shows characteristic changes in the presence of both strong acids and bases of micromolar concentrations. When we add base to the aqueous solution of the compound, the absorption spectrum of the molecule does not show any change in the absorption maxima with respect to its neutral analogue. The absorption spectrum of the molecule in aqueous solutions containing micromolar concentration of a strong acid (HCl) shows a sharp change in the absorption maximum with a blue shift to 302 nm. When we further increase the acidity of the medium, the peak shifts to 298 nm (Figure 6a). This blue shift apparently occurs due to the addition of the proton to the lone pair of the nitrogen atom of the molecule. Similar behavior was previously observed by Zhao et al.[56] for some organic molecules containing nitrogen, where they have shown that the continuous addition of acid can annihilate the ICT totally due to the addition of proton to the system through the lone pair of nitrogen. The mechanism of protonation of the probe is shown in Scheme 3b. The emission spectra of the molecule in aqueous medium both in presence of acid and base show a notable change from their unadulterated analogue. In the presence of very low concentration of acid, the emission peaks of the molecule appear at 395 and 465 nm, respectively. Addition of little more acid to the solution changes the LE and ICT peak positions to 385 and 475 nm, respectively (Figure 6b). In both the cases, the intensity of the first peak is significantly higher than the second one. As mentioned earlier, the shorter wavelength peak has been assigned to the locally excited (LE) state of the molecule and the higher wavelength peak to the ICT state of the probe. After addition of the acid to the medium, the lone pair over the nitrogen atom gets protonated and inhibits the charge transfer to large extent. Hence, the

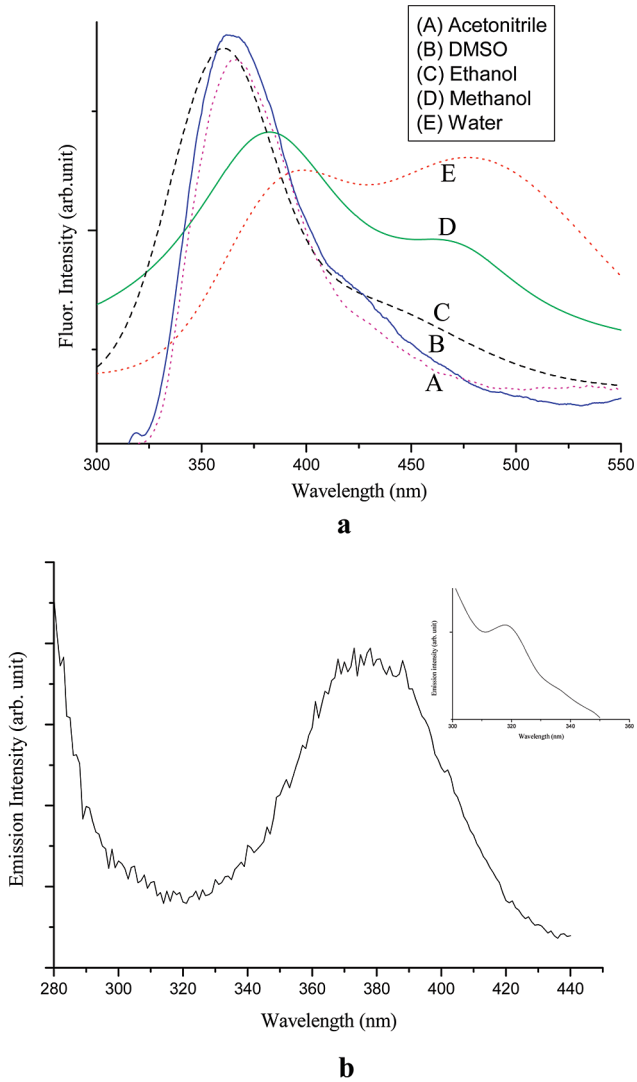

Figure 4. (a) The emission spectra of PACO in acetonitrile, methanol, ethanol, dimethyl sulfoxide (DMSO), and water. The relative intensity of the longer wavelength peak increases from ethanol to methanol to water, with a concomitant decrease in the shorter wavelength peak. The excitation wavelength (λ_{ex}) was 290 nm. (b) The excitation spectra of the probe molecule (PACO) in water with monitoring wavelengtsh of 360 nm (inset) and 450 nm. When monitored at 360 nm (inset), the excitation spectrum matches with the absorption spectra of the probe indicating that the species is generated from the ground state. The excitation spectrum of the probe when monitored at 450 nm does not match with the absorption spectra of the molecule, indicating that the 450 nm species originates in the excited state.

formation of the ICT species decreases and the LE peak shows a higher intensity in the presence of an acid. The stability of the shorter wavelength species in the excited state increases (λ_{max} = 385/395 nm vis-à-vis 380 nm) mainly due to the formation of a charge separated species (Scheme 3c), which is stabilized by water. The key stabilizing factor of the species responsible for the longer wavelength emission is the availability of H^+ ion in the medium, which can be trapped by the negatively charged carbonyl oxygen in the excited state. The explanation remains the same for acids of different concentrations, all in the micromolar region.

The addition of micromolar concentrations of base (NaOH) to the aqueous solution of the probe does not show any change in the absorption maxima. In the presence of micromolar concentrations of base, the emission peaks arise at 355 and 457 nm, respectively. In this case, the intensity of the 457 nm peak is higher than the 355 nm one, which is in complete contrast with what is observed in the presence of acid. The observation can be explained by assuming that the base abstracts the hydrogen atom connected to the nitrogen atom in the probe molecule and promotes the charge transfer process. For this reason, the LE peak intensity decreases with a concomitant increase in the intensity of the ICT peak, as the concentration of the base increases. In the presence of base, the emission spectrum shows that the component that corresponds to the 380 nm peak in water is destabilized and transformed into the species that shows an emission peak at 355 nm. The species corresponding to the 455 nm peak in water is stabilized slightly in the presence of base and a red shift is observed. In acidic solutions, however, both the peaks get red-shifted, implying stability of both the species in the excited state. The pH dependent absorption and emission spectra of the molecule can be best understood with the help of Scheme 3c,d. These observations could have a bearing in designing pH sensors and related applications.[57]

SCHEME 2: The Schematic Energy Diagram Depicting the Formation of the ICT State[a]

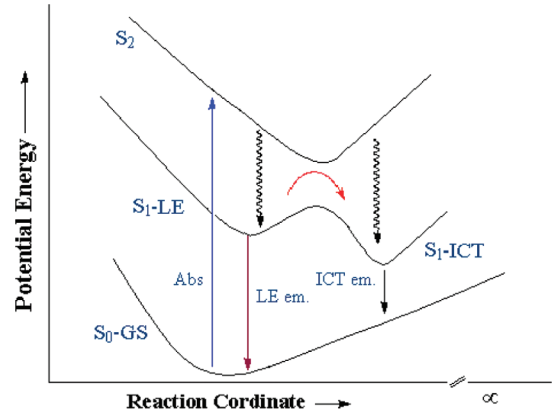

[a] The ground state (S_0-GS) absorbs (Abs) light of suitable wavelength to go to the second excited (S2) state, which has a conical intersection with both the locally excited (S1-LE) and intramolecular charge transfer (S1-ICT) state, from where emissions occur (LE em. and ICT em.). Excitation at wavelengths longer than 320 nm populates the S1-LE state which is converted to the S1-ICT, and we get a single peak from the ICT species (ICT em.).

3f. Low-Temperature (77 K) Emission Spectra of the Probe. From observations made so far, we may propose the following picture. The formation of the excited electronic state is accompanied by an internal conversion (IC) into a new state that has a much larger dipole moment. The normal emission continues during the process. The sudden change in dipole moment (μ), compared to the molecule in the ground state and the significantly different equilibrium geometry trigger a massive solvent reorganization around the excited probe. The solvent reorganization stabilizes the intramolecular charge transfer state strongly and a long wavelength emission sets in from the solvent-stabilized ICT state. At room temperature, the solvent stabilized ICT state may cross over into the normal excited state by solvent fluctuations. As temperature is lowered, the scale of such fluctuations diminishes and the molecule gets entirely trapped in the solvent stabilized ICT state. To put this hypothesis to experimental validation, we have recorded the emission spectrum of PACO in ethanol and 3-methyl pentane glass matrices at 77 K. The recorded fluorescence spectra of the molecule in ethanol and in 3-methyl pentane are displayed in Figure 7. The fluorescence intensities of the probe in ethanol

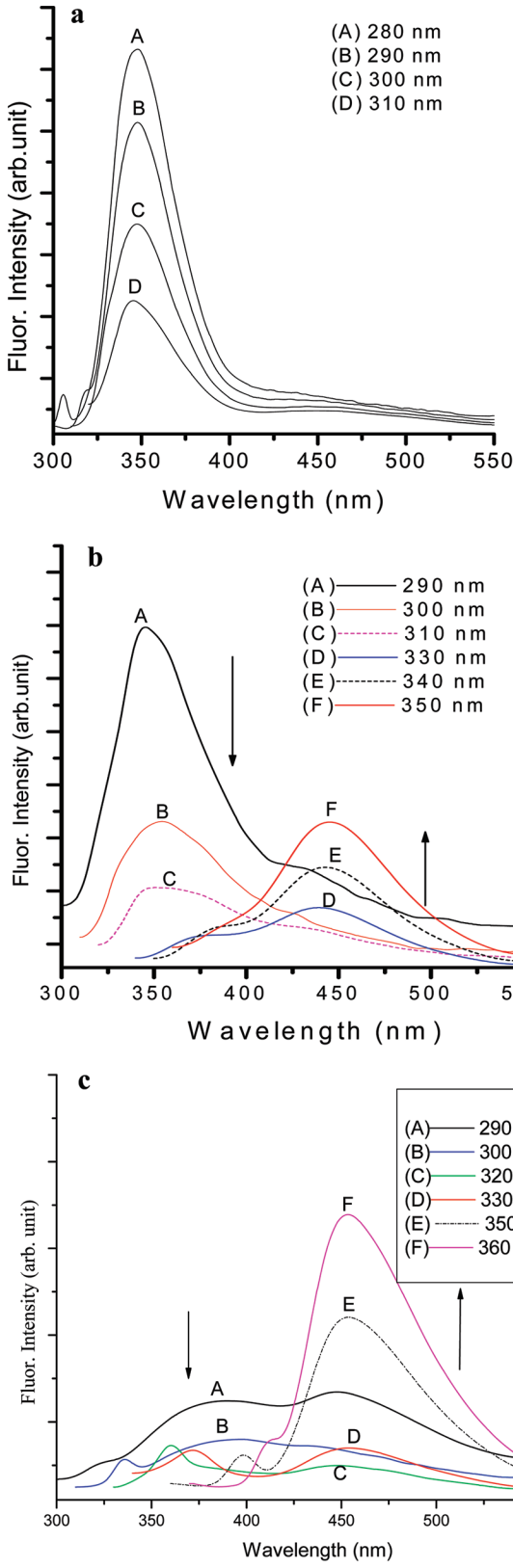

Figure 5. (a) Excitation wavelength dependent spectra of PACO for different excitation wavelength in 1,4-dioxane. (b) Excitation wavelength dependent spectra of PACO in different excitation wavelength in ethanol. With increase in the excitation wavelength, the shorter wavelength peak decreases with a simultaneous increase in the longer wavelength peak. (c) Excitation wavelength dependent spectra of PACO in different excitation wavelength in water. With increase in the excitation wavelength, the shorter wavelength peak intensity decreases with a simultaneous increase in the longer wavelength peak intensity.

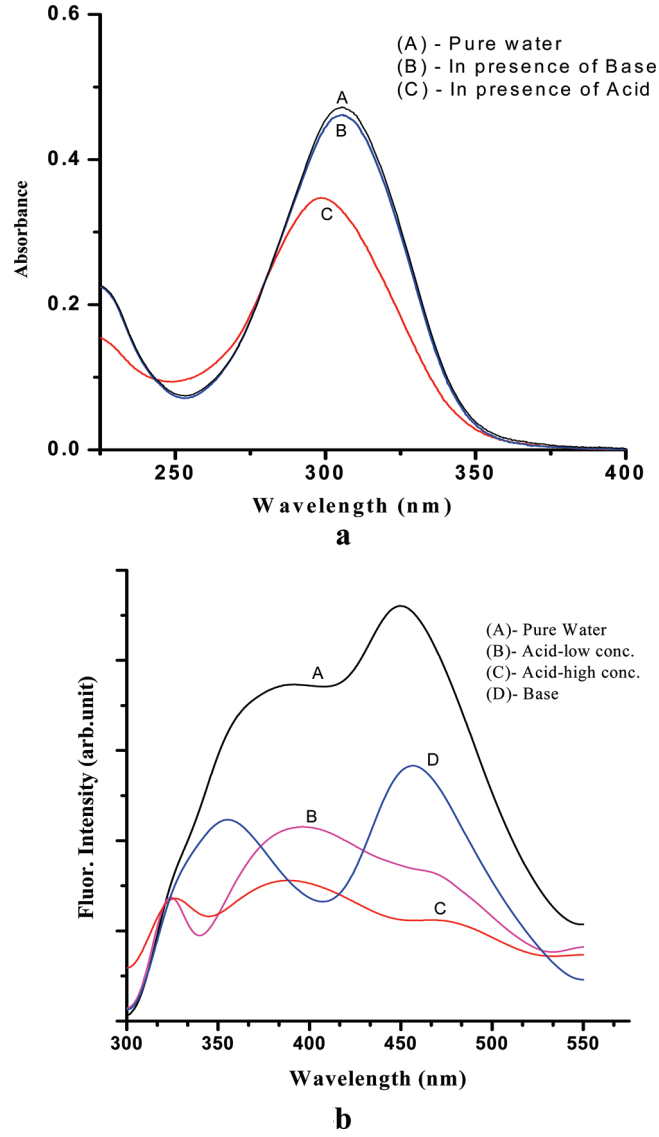

Figure 6. (a) The absorption spectra of the molecule in water in the presence of a dilute acid of micromolar concentrations (HCl) and dilute base (NaOH). In the presence of acid a blue shift of the absorption spectra is observed while the addition of base keeps the absorption maxima unchanged. (b) The emission spectra of PACO in pure water and in the presence of a dilute acid (HCl) of different concentrations and a dilute base (NaOH). The samples were excited (λ_{ex}) at 290 nm. The addition of acid enhances the LE peak intensity with a concomitant decrease in the intensity of ICT peak. The observation is reverse when base is added to the aqueous solution of the probe.

and 3-methyl pentane at 77 K were a hundred times lower than its room temperature counterparts. We note that the dual emission of the probe at room temperature in ethanol at 370 and 440 nm has been replaced by single broad emission band with the peak position slightly red-shifted relative to the long wavelength emission peak (450 nm). A related but qualitatively different observation was made by Ray et al.[58] while recording the emission spectrum of charge transfer probe, 5-(p-dimethylaminobenzyledene)-rhodamine in ethanol at 77 K, and attributed to the absence of solvent relaxation which is hindered at low temperature. The low temperature (77 K) spectrum of the probe molecule in 3-methyl-pentane also shows a single peak at 450 nm (Figure 7). The similarity in the emission spectra of PACO in ethanol and 3-methyl pentane appears to be intriguing at the first sight. The explanation possibly lies in an increase of effective polarity of solvents at low temperature.[59] At low-

SCHEME 3

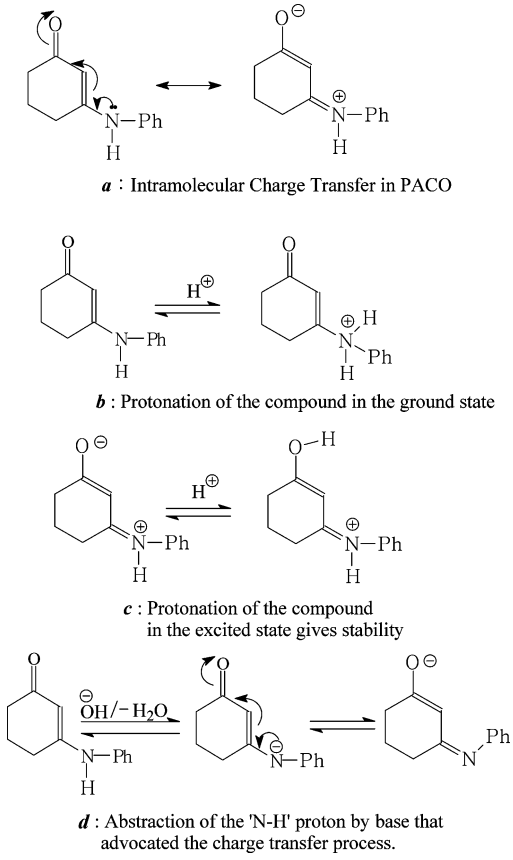

temperatures the scale of thermal fluctuation gets reduced and the viscosity of the solvent increases. There is an enhancement of effective polarity of the solvent with decrease in temperature and the local ordering of solvent molecules increases around the dipolar probe. When the solvent freezes, this enhanced local organization also freezes. A polar solvent remains highly oriented around the dipolar probe even at room temperature and does not reveal much change as the temperature is lowered. For solvents of lower polarity, the increase in local solvent

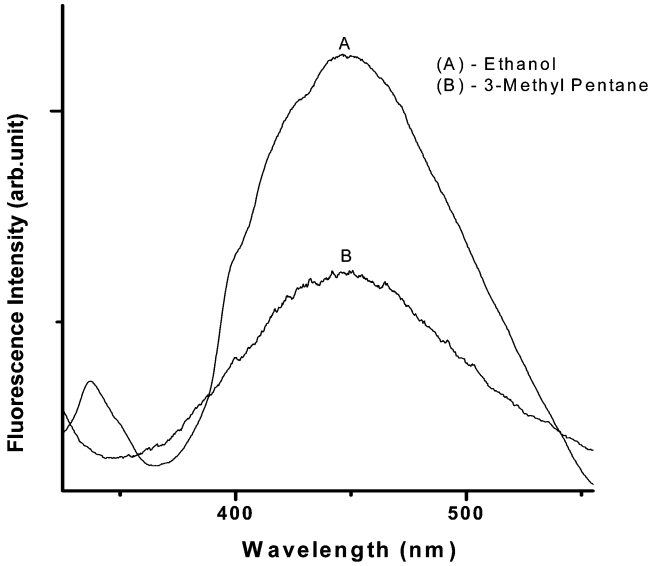

Figure 7. The emission spectra of the probe at 77 K in ethanol (A) and 3-methyl pentane (B). A broad peak at 450 nm arises in both the solvents. The excitation wavelength (λ_{ex}) was 290 nm.

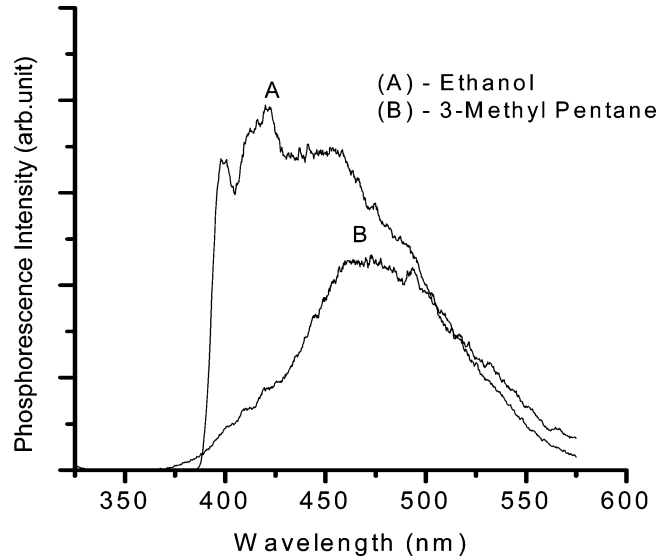

Figure 8. The phosphorescence spectrum of the molecule in ethanol (A) and 3-methyl pentane (B) at 77 K. The samples were excited (λ_{ex}) at 290 nm.

organization at lower temperature appears to be much higher, leading to the observed similarity of the emission spectra in 3-methyl pentane and in ethanol at 77 K.

While recording the low-temperature (77 K) emission spectra of the molecule, we have also recorded the phosphorescence spectra of the molecule at the same temperature. The recorded phosphorescence spectra of the molecule in ethanol and 3-methyl pentane are reported in Figure 8. In ethanol and 1-methyl-pentane glass matrix, the phosphorescence peaks appear at 455 and 470 nm, respectively. It appears that the excited singlet and the triplet lie quite close allowing rather efficient intersystem crossing (ISC).[60,61]

3g. Time Resolved Spectroscopic Analysis. Room temperature time-resolved emission spectra of the molecule in various solvents are displayed in Figure 9a,b. For the time-resolved studies of the probe, the excitation wavelength (λ_{exc}) of 295 nm was used. We have measured the lifetime of the species formed by monitoring the emission at its corresponding steady-state emission wavelengths. The lifetime components we got after fitting the decay curve of the probe in different solvents are displayed in Table 4. Analysis of the decay profile indicates the formation of two distinct species in all the solvents. With triexponential fitting, we get a component in the 10 picosecond (ps) range, which presumably arises due to the solvent reorganization. By monitoring the decay at the corresponding steady state emission peak (335−380 nm), the following results have been obtained.

In every solvent two excited species are formed. In methyl cyclohexane, for example, one species having a lifetime of 1.47 ns with a relative abundance of 90% and the other with a lifetime of 4.5 ns with a relative abundance of 4%, are formed. In isopropyl alcohol, we get two species with lifetimes 3.87 ns (78%) and 15 ns (16%), while in DMSO, the lifetime and abundances of these two components are 5.2 ns (81%) and 22 ns (18%), respectively. In water, the relative abundance of the component with the longest lifetime increases (20%) and the lifetime itself becomes 30 ns, while the lifetime of the other species is 5.41 ns with a relative abundance of 77%. So, it is obvious that the lifetime of the charge transfer state increases as we go from methyl cyclohexane to water, that is, with the increase of dielectric constant of the medium. When the lifetimes

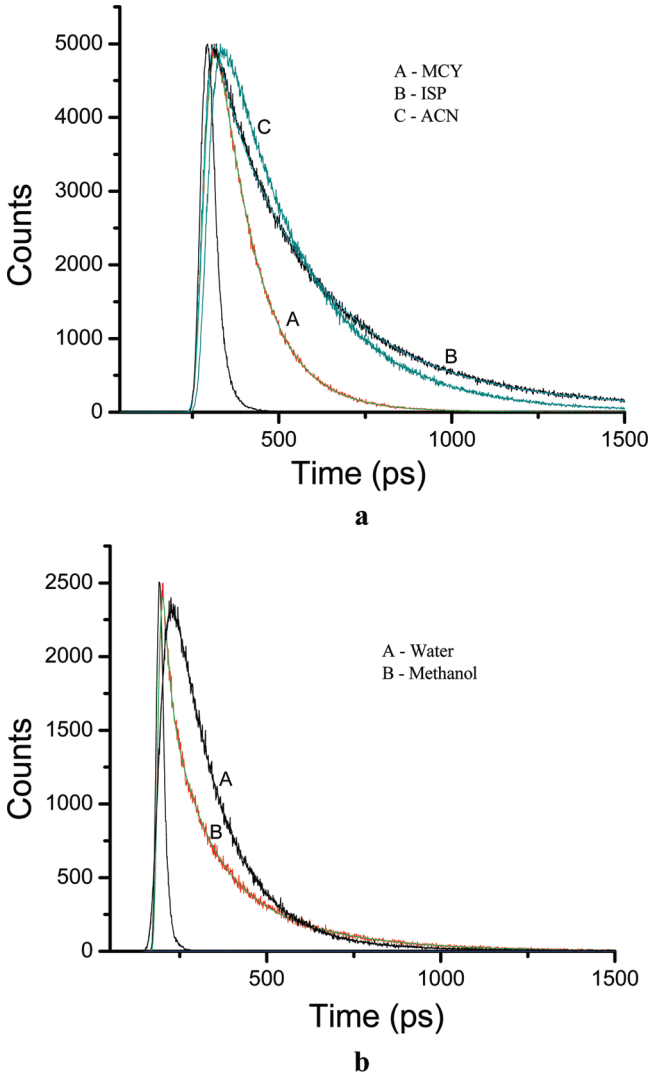

Figure 9. (a) The time-resolved decay profile of PACO in methyl cyclohexane (MCY), isopropyl alcohol (ISP), and acetonitrile (ACN) at 296 K. Emissions were monitored at 334, 372, and 360 nm for methylcyclohexane, isopropanol, and acetonitrile, respectively. Global analysis of the decay and the instrument response function is also shown. (b) The time-resolved decay profile of PACO in methanol and water. Emission wavelengths were monitored at 370 and 380 nm for methanol and water, respectively, at 296 K. Global analysis of the decay and the instrument response function is also shown.

of the probe are measured in methanol and ethanol, an anomalous behavior is observed. The lifetime of the two species formed in methanol are 1.8 and 5.5 ns with a relative abundance of 89% and 6%, respectively. In ethanol, the lifetimes of the two components formed are 2.5 and 8 ns with a relative abundance of 52% and 35%, respectively. In view of the higher dielectric constant of methanol, one would expect the relative abundance of the species responsible for the longer wavelength emission to be higher in methanol than ethanol. When monitored at 440 nm, the lifetime and abundance of the two species in methanol are 1.80 ns (45%) and 7.22 ns (47%), respectively. Here two species appear to be present equally. The lifetimes of the species formed in water have lifetimes of 2.50 ns (31%) and 7.12 ns (59%), respectively. In water, the abundance of the component with larger lifetime probe is much higher than that of the species with smaller lifetime.

The lifetime of the probe in water has been measured also in the presence of acid. The relative abundance of the two species shows a similar behavior as was observed in the steady state emission spectra of the sample, that is, the higher intensity of the lower wavelength species (LE) over the species with higher wavelength (ICT). The lifetime (λ_{mon} = 385 nm) of the LE species is 2 ns with a relative abundance of 79% and 8.4 ns with a relative abundance of 12% for the ICT species. Interestingly, the lifetimes of both the species are noticeably much lower than those in pure water. Thus, we have observed fluorescence quenching of the probe in two apparently different media, viz., in alcoholic solvents, methanol and ethanol, and in aqueous solutions in the presence of micromolar concentration of acid. The quenching of fluorescence is more pronounced in methanol than that in ethanol, although the former has a higher dielectric constant. Now, we can relate these two observations. As we have mentioned earlier, methanol has higher hydrogen-bond donor ability than ethanol, so an inference can be drawn that in the excited state the probe possibly abstracts proton from ethanol and methanol. This leads to the quenching of the fluorescence, and more so in methanol than in ethanol.

3h. Quantum Yield, Radiative and Nonradiative Rates. Table 5a reports the radiative and nonradiative rate constants (k_r and k_{nr}, respectively) obtained from the emission spectra of the probe in different solvents. The measured steady state fluorescence quantum yield (ϕ) is related to the radiative rate constant (k_r) and (k_{nr}) by the following equation:

$$\phi = \frac{k_r}{k_r + k_{nr}}$$

The observed decay time (τ) is given by

TABLE 4: The Lifetime of Each Species (in Nanosecond) at the Monitoring Wavelength (λ_{mon}) of the Probe in Different Solvents[a]

	lifetimes (λ_{mon} = 340−360 nm)			lifetimes (λ_{mon} = 440−450 nm)		
medium	τ_1 (ns)	τ_2 (ns)	τ_3 (ns)	τ_1 (ns)	τ_2 (ns)	τ_3 (ns)
(i) methyl cyclohexane	0.04 (6)	1.47 (90)	4.5 (4)			
(ii) acetonitrile	0.01 (3)	3.1 (91)	6.0 (6)			
(iii) isopropanol	0.23 (6)	3.9 (78)	15 (16)			
(iv) ethanol	0.46 (8)	2.7 (70)	12 (22)	0.23 (12)	2.5 (52)	8 (35)
(v) methanol	0.14 (5)	1.8 (89)	4.7 (6)	0.2 (9)	1.9 (51)	7 (40)
(vi) DMSO	0.2 (1)	5.2 (81)	22 (17)	0.1 (13)	2.4 (21)	7.7 (59)
(vii) water	0.9 (3)	5.4 (77)	30 (20)	0.16 (10)	2.5 (31)	7.1 (59)
(viii) water + dilute acid	0.2 (9)	2 (79)	8.4 (12)	0.6 (6)	2.5 (78)	9.3 (16)

[a] The sample was excited at 295 nm. The numbers in the parentheses represent the relative contribution of the species in percentage (%) scale. The χ^2 values vary from 0.86 to 1.12.

$$\tau = \frac{1}{k_r + k_{nr}}$$

These two quantities lead directly to the values of k_r and k_{nr} that are supposed to characterize the emission process.

The oscillator strength has been computed from the recorded absorption spectra using the expression[42]

$$f = \frac{4.39 \times 10^{-9}}{n} \int \varepsilon(\bar{v})\, d\bar{v}$$

where $\int\varepsilon(\bar{v})$ is the molar absorption coefficient at frequency $d\upsilon$, and n is the refractive index of the medium. The area under the curve from 250 to 400 nm was computed leading to the value of the integral.

The radiative lifetime (τ_r) has been determined from the absorption spectrum by using the equation[62]

$$\tau_r = \frac{2\pi\varepsilon_0 m_0 c^3}{ne^2\omega^2 f}$$

where ε_0, m_0, and c are the permittivity of the vacuum, rest mass of electron, and speed of light, respectively, n is the refractive index of the media, e is the charge of electron, ω is the frequency of the transition, and f is the oscillator strength of the transition. Inversion of the radiative lifetime (τ_r) gives the radiative rate constant (k_r) of the transition. The results obtained for different solvents are reported in Table 5a.

TABLE 5

(5a) The radiative and nonradiative rate constants obtained from absorption and emission spectra of the molecule

solvent	$(k_r)_{LE}$ from emission ($\times 10^5$ s^{-1})	$(k_{nr})_{LE}$ from emission ($\times 10^8$ s^{-1})	k_r from absorption ($\times 10^{11}$ s^{-1})
methylcyclohexane	40.8	6.78	5.60
ethanol	36.0	3.69	4.95
methanol	83.0	9.85	4.80
DMSO	8.30	4.16	5.30
water	2.03	1.79	4.69

(5b) Experimental oscillator strengths of absorption (f) and emission (f_{fl}) of PACO in different solvents

solvents	oscillator strength (abs)	oscillator strength (emm) ($\times 10^{-3}$)
methylcyclohexane	0.521	6.8
ethanol	0.520	6.5
methanol	0.510	17
DMSO	0.514	1.6
water	0.504[a]	0.44

(5c) The excitation energies and oscillator strengths of transition as obtained with TDDFT calculation (mPW1PW91 functional) using the AM1 excited state optimized geometry, employing cc-pVTZ basis set

transition	transition energy (nm)	oscillator strength
HOMO−LUMO	1205.26	0.0008
[HOMO − 1]−LUMO	455.30	0.0327
HOMO−[LUMO + 1]	387.44	0.0416

[a] Theoretically calculated oscillator strength of the $S_0 \rightarrow S_2$ transition computed with TDDFT/B3LYP = 0.4956 and with TDDFT/mPW1PW91 = 0.5031, employing cc-pVTZ basis set.

SCHEME 4[a]

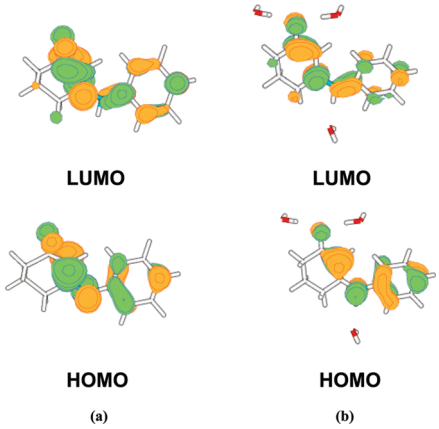

[a] HOMO and LUMO of (a) the bare molecule (PACO) and (b) microcluster of PACO and three water molecules, calculated by B3LYP hybrid density functional theory employing cc-pVTZ basis set as implemented in GAMESS. The contour plots are drawn with the maximum contour value of 0.07 following MOLDEN visualization program.

Table 5b reports the experimentally observed oscillator strengths of the absorption and the emission processes in different solvents. The oscillator strength of the fluorescence (f_{fl}) has been calculated with the help of the equation[63]

$$f_{fl} = \frac{1.499}{\upsilon_0^{\,2}\tau_r}$$

where ν_0 is the fluorescence transition energy in cm^{-1} and τ_r is the radiative lifetime of the emitting species (in seconds).

The rather low oscillator strength predicted for emission (of the order of 10^{-3}) vis-à-vis the absorption (of the order of 0.5) indicates that absorption of light populates a state which is not the emitting state, a fact that is also reflected in the widely different values of k_r (emission) and k_r (absorption). The experimental oscillator strengths of absorption in different solvents are around 0.50, which is similar to that we have obtained theoretically for the S_0-S_2 transition of PACO in water. From the values of oscillator strength[64,65] for absorption and emission we can speculate that the emission takes place from an $n\pi^*$ state, while the absorption involves a $\pi\pi^*$ transition. Our TDDFT (mPW1PW91 functional) based prediction of transition energies (Table 5c) at the AM1 excited state optimized geometry support our experimental observation. The method yields low oscillator strength for the first three transitions, all strongly red-shifted with respect to the first three transitions seen in absorption.

3i. Structure of the ICT State. From ab initio calculations, it turns out that the singlet state corresponding to the HOMO to LUMO transition dominates the computed absorption spectral profile (the oscillator strength is the largest). The figures of HOMO and LUMO can therefore provide us with some idea about the nature of the excited state involved in the ICT process. Scheme 4 displays the HOMO and LUMO of the bare PACO molecule and the PACO.3H_2O microcluster. It is clear that the transition involves significant transfer of electron density from the aromatic ring to the cyclohexen-1-one moiety and more so when the molecule is microsolvated in water. It would be relevant and useful to have some idea about the molecular structure of PACO in the excited state.

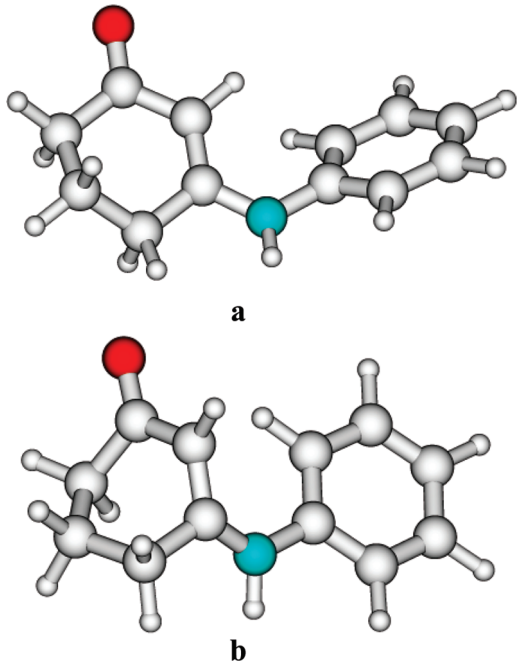

Figure 10. (a) The AM1-optimized geometry of the molecule in the ground state. The geometry of the molecule was optimized using configuration interaction (C.I.) = 2. (b) The AM1 optimized geometry of the molecule in the excited state. C.I. = 2 was used for geometry optimization.

Ab-initio geometry optimization of the molecule in the excited state proved to be costly. Austin model 1 (AM1) has been known to predict structures of ground and low-lying excited state fairly well at low computational cost. Hofkens et al.[66] have used AM1/CI technique to optimize the ground and first excited singlet and triplet states of peryleneimide molecules and compared the results obtained with coupled cluster singles and doubles and reported that the two methods yield similar results. Soujanya[67] et al. have performed AM1 calculations on two different charge transfer probes, viz., 4-amino pthalimide (AP) and 4-(*N*,*N*-dimethylamino)-pthalimide (DAP) and concluded that AM1 level of theory could be helpful in computing geometries and dipole moments of the molecules in both the ground and excited states. The experimentally determined change in dipole moment associated with the transition into the excited state matches closely with that predicted at this level of theory. We have already seen that for the present molecule, the predicted ground state geometrical parameters and dipole moment computed at the AM1 level match well with the ab initio theoretical data. We may, therefore, have some confidence in the AM1 predicted structure of the excited state. We carried out complete geometry optimization of the molecule in both the S_0 and S_1 states using the limited CI (singles and doubles involving HOMO and LUMO) option at the AM1 level of approximation. The optimized structures for the S_0 and S_1 states are shown in Figure 10 panels a and b, respectively. The geometries are significantly different in the two states and the dipole moment in the S_1 state (10.60 D) is predicted to be much higher than in the S_0 state (4.50 D). The dipole moment of the S_0 state predicted by the B3LYP calculation is 5.60 D. There is strong evidence of charge transfer from the nitrogen atom along the π-conjugative network $N_8-C_7=C_4-C_1=O_3$ upon excitation (Table 6a). The charges in the excited state were computed by performing calculations at the restricted Hartree−Fock level at the configuration interaction (C.I.) optimized geometry. The bond lengths between pairs of the atoms in the charge transfer path shows (Table 6b)

TABLE 6

(6a) The ground and excited state charge distribution (in electronic unit) over the atoms of the molecule, calculated by AM1 level of approximation using C.I. = 2

	atoms				
	N_8	C_7	C_4	C_1	O_3
ground state	−0.267	0.104	−0.339	0.275	−0.314
excited state	0.023	0.305	−0.778	0.190	−0.407

(6b) The bond lengths (Å) between different atom pairs in the compound both in ground state and excited state, calculated by AM1 level of approximation using C. I. = 2 option

	bond lengths (Å)			
	N_8-C_7	C_7-C_4	C_4-C_1	C_1-O_3
ground state	1.39	1.36	1.46	1.23
excited state	1.34	1.41	1.42	1.24

that following the excitation, the N_8-C_7 bond length has substantially decreased while the C_7-C_4 bond length has increased. The C_4-C_1 bond length also decreases substantially without, however, affecting the C_1-O_3 bond which retains its normal length. The net charge on O_3, however, increases substantially in the excited state. These bond length changes are compatible with the HOMO and LUMO pictures, shown in Scheme 4. It appears reasonable therefore to identify the S_1 state as the state ultimately responsible for the ICT emission on photoexcitation.

4. Conclusions

The molecule (PACO) has a low-lying strongly polar excited singlet state which has the characteristics of an intramolecular charge transfer (ICT) state. The dual fluorescence in polar solvents together with the pH dependent study, that is, effect of increasing acidity and basicity of the medium on the absorption and emission characteristics of the probe and the low temperature emission study characterizes the species responsible for the emission in the longer wavelength as the ICT state of PACO. The dielectric constants of the solvents play a major role in stabilizing the polar exited state of the molecule. A decrease in charge transfer was observed in the presence of micromolar concentration of acids, which helps in predicting the charge distribution pathway in the excited state. The quenching of fluorescence in presence of acids and in alcoholic solvents, viz., ethanol and methanol leads us to conjecture that the probe abstracts proton from these solvents in the excited state. The experimentally obtained oscillator strengths of the absorption and the emission indicate that absorption and emission occur from different states. The role of both macroscopic as well as microscopic solvation in the ICT process was studied using quantum chemical ab initio calculations. Theoretical predictions of the absorption spectrum of the probe in different media reveal strong effects of microscopic as well as macroscopic solvation in stabilizing the ICT state. The 1:3 micromolecular cluster of PACO with water emerges as an important species, which deserves further exploration for a more complete understanding of the ICT state and mechanism.

Acknowledgment. Sincere thanks to Prof. S. C. Roy and Dr. Biplab Banerjee, Department of Organic Chemistry, IACS for their help during synthesis of the molecule. We thank Dr. Paulami Mandal and Prof. T. Ganguli, Department of Spectroscopy for the low temperature studies and Mr. Subrata Das

for time-resolved studies. R.M. is grateful to Mr. Partha Roy for technical help and the integrated Ph.D. division, IACS, for financial support.

References and Notes

(1) Sedghi, G.; Sawada, K.; Esdaile, L. J.; Hoffmann, M.; Anderson, H. L.; Bethell, D.; Haiss, W.; Higgins, S. J.; Nichols, R. J. *J. Am. Chem. Soc.* **2008**, *130*, 8582.
(2) Closs, G. L.; Miller, J. R. *Science* **1988**, *240*, 440.
(3) Barbara, P. F.; Walker, G. C.; Smith, T. P. *Science* **1992**, *256*, 975.
(4) Kobori, Y.; Yamauchi, S.; Akiyama, K.; Tero-Kubota, S.; Imahori, H.; Fukuzumi, S.; Norris, J. R. *Proc. Natl. Acad. Sci. U.S.A.* **2005**, *102*, 10017.
(5) Zhao, G.-J.; Liu, J.-Y.; Zhou, L.-C.; Han, K.-L. *J. Phys. Chem. B* **2007**, *111*, 8940.
(6) Bulheller, B. M.; Miles, A. J.; Wallace, B. A.; Hirst, J. D. *J. Phys. Chem B* **2008**, *112*, 1866.
(7) Li, G.; Josowicz, M.; Janata, J.; Semancik, S. *Appl. Phys. Lett.* **2004**, *85*, 1187.
(8) Arzhantsev, S.; Zachariasse, K. A.; Maroncelli, M. *J. Phys. Chem. A* **2006**, *110*, 3454.
(9) Cao, X.; Tolbert, R. W.; McHale, J. L.; Edwards, W. D. *J. Phys. Chem. A* **1998**, *102*, 2739.
(10) Thar, J.; Zahn, S.; Kirchner, B. *J. Phys. Chem. B* **2008**, *112*, 1456.
(11) Akemann, W.; Laage, D.; Plaza, P.; Martin, M. M.; Blanchard-Desce, M. *J. Phys. Chem. B* **2008**, *112*, 358.
(12) Zyss, J.; Ledoux, I.; Volkov, S.; Chernyak, V.; Mukamel, S.; Bartholomew, G. P.; Bazan, G. C. *J. Am. Chem. Soc.* **2000**, *122*, 11956.
(13) Zachariasse, K. A. *Chem. Phys. Lett.* **2000**, *320*, 8.
(14) Rettig, W.; Bliss, B.; Dirnberger, K. *Chem. Phys. Lett.* **1999**, *305*, 8.
(15) Rettig, W. *Angew. Chem., Int. Ed. Engl.* **1986**, *25*, 971.
(16) Zilberg, S.; Haas, Y. *J. Phys. Chem. A* **2002**, *106*, 1.
(17) Yoshihara, T.; Druzhinin, S. I.; Zachariasse, K. A. *J. Am. Chem. Soc.* **2004**, *126*, 8535.
(18) Gomez, I.; Reguero, M.; Boggio-Pasqua, M.; Robb, M. A. *J. Am. Chem. Soc.* **2005**, *127*, 7119.
(19) Cogan, S.; Zilberg, S.; Haas, Y. *J. Am. Chem. Soc.* **2006**, *128*, 3335.
(20) Datta, A.; Mandal, D.; Pal, S. K.; Bhattacharyya, K. *J. Phys. Chem. B* **1997**, *101*, 10221.
(21) Barbatti, M.; Aquino, A. J. A.; Lischka, H.; Schriever, C.; Lochbruner, S.; Riedle, E. *Phys. Chem. Chem. Phys.* **2009**, *11*, 1406.
(22) Ameer-Beg, S.; Ormson, S. M.; Matousek, P.; Towrie, M.; Nibbering, E. T. J.; Foggi, P.; Neuwhal, F. V. R. *J. Phys. Chem. A* **2001**, *105*, 3709.
(23) Mitra, S.; Das, R.; Bhattacharyya, S. P.; Mukherjee, S. *J. Phys. Chem. A* **1997**, *101*, 293.
(24) Tarakeswar, P.; Kim, K. S.; Djafari, S.; Buchhold, K.; Reimann, B.; Barth, H.-D.; Brutschy, B. *J. Chem. Phys.* **2001**, *114*, 4016.
(25) Miyazaki, M.; Fujii, A.; Ebata, T.; Mikami, N. *Science* **2004**, *304*, 1134.
(26) Dickinson, J. A.; Hockridge, M. R.; Kroemer, R. T.; Robertson, E. G.; Simons, J. P.; McCombie, J.; Walker, M. *J. Am. Chem. Soc.* **1998**, *120*, 2622.
(27) Pathak, A. K.; Mukherjee, T.; Maity, D. K. *J. Chem. Phys.* **2006**, *124*, 024322.
(28) Brutschy, B. *Chem. Rev.* **2000**, *100*, 3891.
(29) Reiman, B.; Buchhold, K.; Vaupel, S.; Brutschy, B.; Havlas, Z.; Spirko, V.; Hobza, P. *J. Phys. Chem A* **2001**, *105*, 5560.
(30) Pal, S. K.; Peon, J.; Zewail, A. H. *Proc. Natl. Acad. Sci. U.S.A.* **2002**, *99*, 1763.
(31) Ramtohul, Y. K.; Chartrand, A. *Org. Lett.* **2007**, *9*, 1029.
(32) Dondoni, A.; Perrone, D. *Synthesis* **1993**, 1162.
(33) Bell, I. M.; Erb, J. M.; Freidinger, R. M.; Gallicchio, S. N.; Guare, J. P.; Guidotti, M. T.; Halpin, R. A.; Hobbs, D. W.; Homnick, C. F.; Kuo, M. S.; Lis, E. V.; Mathre, D. J.; Michelson, S. R.; Pawluczyk, J. M.; Pettibone, D. J.; Reiss, D. R.; Vickers, S.; Williams, P. V.; Woyden, C. J. *J. Med. Chem.* **1998**, *41*, 2146.
(34) Scott, K. R.; Edafiogho, I. O.; Richardson, E. L.; Farrar, V. A.; Moore, J. A.; Tietz, E. I.; Hinko, C. N.; Chang, H.; El-Assadi, A.; Nicholson, J. M. *J. Med. Chem.* **1993**, *36*, 1947.
(35) Caprathe, B. W.; Jaen, J. C.; Wise, D. L.; Heffner, T. G.; Pugsley, T. A.; Meltzer, L. T.; Parvez, M. *J. Med. Chem.* **1991**, *34*, 2736.
(36) Gatta, F.; Guidice, M. R. D.; Pomponi, M.; Marta, M. *Heterocycles* **1992**, *34*, 991.
(37) Dal Pozzo, R.; De Nino, A.; Nardi, M.; Russo, B.; Procopio, A. *Synthesis* **2006**, *62*, 611.
(38) Paira, M.; Misra, R.; Roy, S. C. *Indian J. Chem.* **2008**, *47B* (6), 966.
(39) Epifano, F.; Genevese, S.; Curini, M. *Tetrahedron Lett.* **2007**, *48*, 2717.
(40) Calle, M.; Calvo, L. A.; Gonzales-Ortega, A.; Gonzales-Nogal, A. *Tetrahedron* **2006**, *62*, 611.
(41) Dewar, M. J. S.; Zoebisch, E. G.; Healy, E. F.; Stewart, J. J. P. *J. Am. Chem. Soc.* **1985**, *107*, 3902.
(42) Lakowicz, J. R. *Principle of Fluorescence Spectroscopy,* 3rd ed.; Springer: New York, 2006, Chapters 1−3.
(43) Schmidt, M. W.; Baldridge, K. K.; Boatz, J. A.; Elbert, S. T.; Gordon, M. S.; Jensen, J. H.; Koseki, S.; Matsunaga, N.; Nguyen, K. A.; Su, S.; Windus, T. L.; Dupuis, M.; Montgomery, M. A. *J. Comput. Chem.* **1993**, *14*, 1347.
(44) Schaftenaar, G.; Noordik, J. H. *J. Comput.-Aided. Mol. Des.* **2000**, *14*, 123.
(45) Jamorski, C.; Foresman, J. B.; Thilgen, C.; Luthi, H-.P. *J. Chem. Phys.* **2002**, *116*, 8762.
(46) Lippert, E.; Luder, W.; Moll, F.; Nagele, W.; Boos, H.; Prigge, H.; Seibold-Blankenstein, I. *Angew. Chem.* **1961**, *73*, 695.
(47) Demeter, A.; Berces, T.; Zachariasse, K. A. *J. Phys. Chem. A* **2001**, *105*, 4611.
(48) Cornelissen-Gude, C.; Rettig, W. *J. Phys. Chem. A* **1998**, *102*, 7754.
(49) Kamlet, M. J.; Abboud, J. L. M.; Abraham, M. H.; Taft, R. W. *J. Org. Chem.* **1983**, *48*, 2877.
(50) Hattig, C.; Hellwey, A.; Kohn, A. *J. Am. Chem. Soc.* **2006**, *128*, 15672.
(51) Gomez, I.; Mereier, Y.; Reguero, M. *J. Phys. Chem. A* **2006**, *110*, 11455.
(52) Adhikari, R. M.; Neckers, D. C. *J. Phys. Chem. A* **2009**, *113*, 417.
(53) Oakley, M. T.; Guichard, G.; Hirst, J. D. *J. Phys. Chem. B* **2007**, *111*, 3274.
(54) Dreuw, A.; Weisman, J. L.; Head-Gordon, M. *J. Chem. Phys.* **2003**, *119*, 2943.
(55) Dias, F. B.; Pollock, S.; Hedley, G.; Pålsson, L.-O.; Perepichka, A. M. I.; Perepichka, I. F.; Tavasli, M.; Bryce, M. R. *J. Phys. Chem. B* **2006**, *110*, 19329.
(56) Zhao, G. J.; Chen, R.-K.; Sun, M. T.; Liu, J.-Y.; Li, G.-Y.; Gao, Y.-L.; Han, K.-L.; Yang, X-. C.; Sun, L. *Chem.—Eur. J.* **2008**, *14*, 6935.
(57) Chen, L.; McBranch, D. W.; Wang, H.-L.; Helgeson, R.; Wudl, F.; Whitten, D. G. *Proc. Natl. Acad. Sci. U.S.A.* **1999**, *96*, 12287.
(58) Ray, J.; Panja, N.; Nandi, P. K.; Martin, J. J.; Jones, W.E. Jr. *J. Mol. Struct.* **2008**, *874*, 121.
(59) Bublitz, G. U.; Boxer, S. G. *J. Am. Chem. Soc.* **1998**, *120*, 3988.
(60) Yu, J.-K.; Cheng, Y.-M.; Hu, Y. H.; Chou, P.-T.; Chen, Y.-L.; Lee, S.-W.; Chi, Y. *J. Phys. Chem. B* **2004**, *108*, 19908.
(61) Ramesdonk, H. J.; Bakker, B. H.; Groeneveld, M. M.; Verhoeven, J. W.; Allen, B. D.; Rostron, J. P.; Harriman, A. *J. Phys. Chem. A* **2006**, *110*, 13145.
(62) Shan, W.; Xie, X. C.; Song, J. J.; Goldenberg, B. *Appl. Phys. Lett.* **1995**, *67*, 2512.
(63) Nakamura, T.; Takeuchi, S.; Suzuki, N.; Tahara, T. *Chem. Phys. Lett.* **2008**, *465*, 212.
(64) Kenfack, C. A.; Burger, A.; Mly, Y. *J. Phys. Chem. B* **2006**, *110*, 26327.
(65) Fujino, T.; Arzhantsev, S. Y.; Tahara, T. *J. Phys. Chem. A* **2001**, *105*, 8123.
(66) Hopkens, J.; Cotlet, M.; Vosch, T.; Tinnefeld, P.; Weston, K. D.; Ego, C.; Grimsdale, A.; Mullen, K.; Beljonne, D.; Bredas, J. L.; Jordens, S.; Schweitzer, G.; Sauer, M.; Schryver, F. D. *Proc. Natl. Acad. Sci. U.S.A.* **2003**, *100*, 13146.
(67) Soujanya, T.; Fessenden, R. W.; Samanta, A. *J. Phys. Chem.* **1996**, *100*, 3507.

JP9009542